Glioportal: a comprehensive transcriptomic resource unveiling ligand-mediated mesenchymal transition in glioblastoma

Neuro-Oncology
XX(XX), 1–18, 2025 | https://doi.org/10.1093/neuonc/noaf145 | Advance Access date 16 June 2025

Glioportal: a comprehensive transcriptomic resource unveiling ligand-mediated mesenchymal transition in glioblastoma

Qing You Pang[†], Wisna Novera[†], Lynnette Wei Hsien Koh, Yuk Kien Chong, See Wee Lim, Ngak Leng Sim, Simone Rizzetto, Jinyue Liu, Xuling Lin, Samantha Ya Lyn Ang, Justin Rui-Xin Ker, Kai-Rui Wan, David Chyi Yeu Low, Marija Cvijovic, Wilson Wen Bin Goh, Huilin Shao, Nguan Soon Tan, Stephen Yip, Anders Martin Jacobsen Skanderup, Carol Tang, Patrick Tan,[*] and Beng Ti Ang[*]

All author affiliations are listed at the end of the article

[†]These authors contributed equally.

[*]**Corresponding Authors:** Beng Ti Ang, Neuro-Oncology Research Laboratory, Department of Research, National Neuroscience Institute, Singapore 308433 (ang.beng.ti@singhealth.com.sg), Patrick Tan, Cancer and Stem Cell Biology Program, Duke-National University of Singapore Medical School, Singapore 169857 (gmstanp@duke-nus.edu.sg).

Abstract

Background. Multi-omics profiling of glioblastoma (GBM) has unraveled two aspects fundamental to its aggressiveness and lethality that is molecular heterogeneity inherent to the tumor and cellular plasticity modulated by the microenvironment. Yet, empirical validation to identify causal factors for these complex mechanisms is rather scarce. Here, we report our endeavor in establishing Glioportal, a GBM tumor biobank with derivative preclinical models and molecular information that we leverage for basic and translational research on precision therapies.

Methods. Bulk transcriptome and single-cell-based deconvolution analyses highlighted key features of distinct GBM subtypes and ligand-receptor pairs predicted to regulate malignant cell state plasticity. Synthetic genetic tracing tool and target genes/proteins expression analyses validated ligands-induced mesenchymal transition. This was further corroborated with phenotypic invasion/migration assays and cell-based assays using inhibitors, functional antibodies, and gene silencing approaches. A proof-of-concept animal experiment was conducted using orthotopic xenograft carrying gene knockdown. Clinical relevance was assessed through immunohistochemical assay.

Results. Our transcriptomic analysis highlights the integral roles of STAT3 and NF-κB pathways in maintaining intrinsic mesenchymal identity and enabling myeloid-induced plasticity towards mesenchymal phenotype. One critical ligand, TNF, confers mesenchymal adaptation and cellular invasiveness that is mitigated by TNFRSF1A, but not TNFRSF1B, loss of function. *TNFRSF1A* silencing significantly improves survival in vivo.

Conclusion. Glioportal makes a valuable resource for identifying therapeutic vulnerabilities in molecularly stratified GBM. Here, we underscore GBM dependency on myeloid-derived ligands to acquire mesenchymal traits that have clinical implications in therapeutic response and recurrence. Such reliance warrants treatment strategies targeting ligand-receptor pairs to mitigate interactions with the tumor ecosystem.

Key Points

- Transcriptomic profiling uncovers essential molecular factors governing GBM subtype identity.
- Tumour microenvironment modulates GBM cell plasticity *via* ligand-receptor pair interactions.
- Ligand-receptor pairs present potential actionable therapeutic targets for GBM.

Graphical Abstract

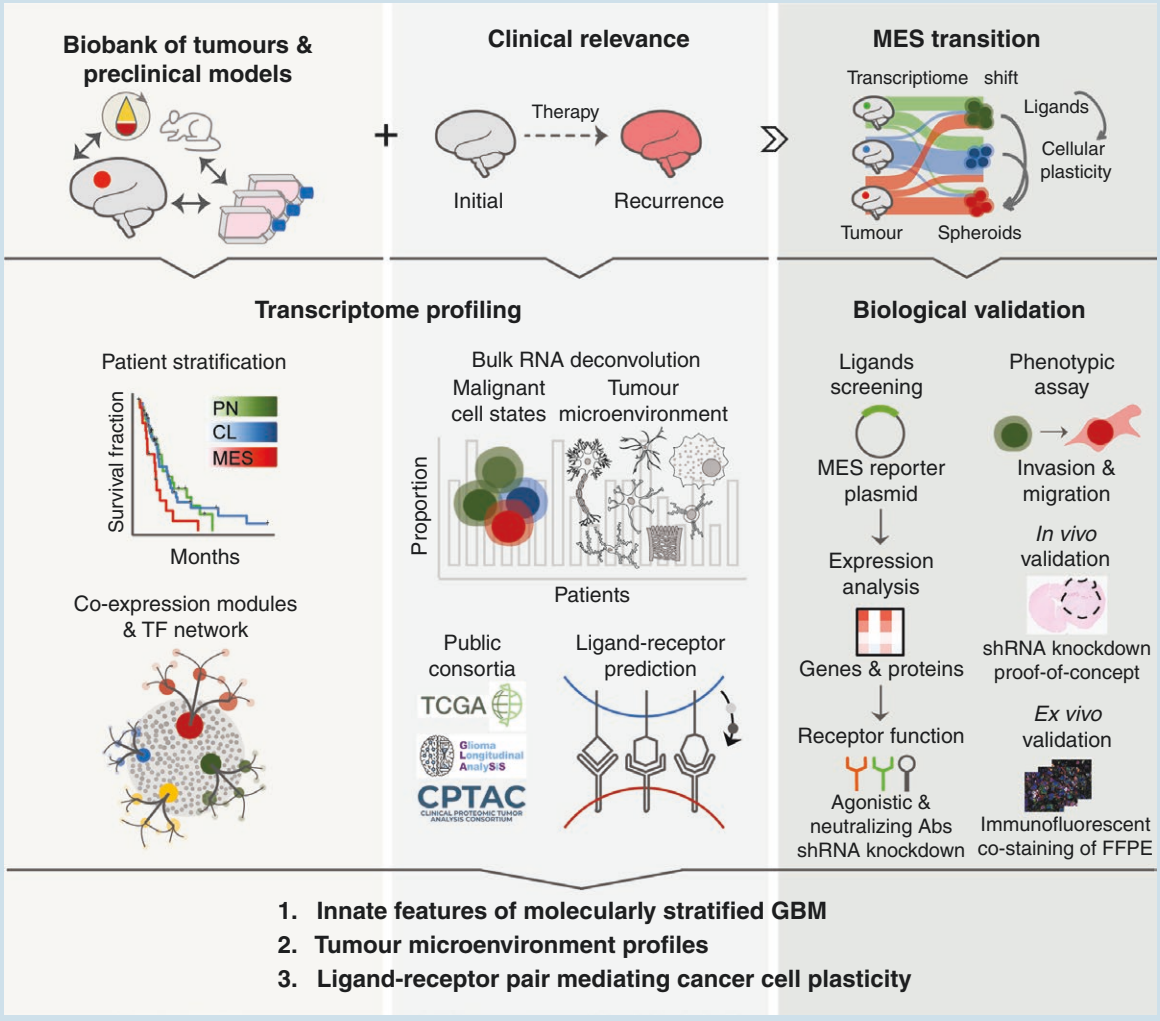

Importance of the Study

This study emphasizes the importance of biological and molecular resources for clinical data-driven hypothesis testing that could benefit prospective cohorts of GBM patients. We established a Glioportal repository, where we continually bank primary tumor tissues and associated fluids, generate derivative patient avatars, as well as curate clinico-pathological and transcriptomic information. Focusing on the mesenchymal GBM subtype often associated with disease recurrence and resistance to therapy, we unraveled their inherent reliance on STAT3 and NF-κB pathways and cross-talk with infiltrating myeloid populations *via* TNF-TNFRSF1A ligand-receptor interaction. These molecular dependencies present therapeutic vulnerabilities that can be potentially targeted.

Glioblastoma (GBM) is the most common primary malignant brain tumor in adults, notorious for its poor prognosis.[1] Despite aggressive therapeutic interventions by maximum surgical resection followed by temozolomide (TMZ) and radiotherapy, the median survival remains less than 15 months.[2] GBM invariably recurs as the tumor regrows from residual cells that already infiltrated surrounding brain tissues beyond the resection margins. Consortia efforts have characterized GBM across clinical, genomic, transcriptomic, epigenomic, proteomic, and anatomical features,[3–6] defining three molecular subtypes, namely, proneural (PN), classical (CL), and mesenchymal (MES). Each subtype arises from distinct lineages and is molecularly governed by specific genetic drivers.[3,4,6,7] Clinically, they vary in prevalence, prognosis, and response to therapy.[6]

The advance of single-cell sequencing and *in silico* methods to deconvolute bulk RNA sequencing data have

Neuro-Oncology

unraveled molecular heterogeneity of GBM that not only occurs between tumors, but also within. Further adding to the complexity is a phenomenon of cell state plasticity, where malignant cells acquire new phenotypes without changing their genetic blueprints.[7,8] One notable example is mesenchymal transition frequently detected in recurrence and clinically correlates with the worst prognostic outcomes.[3,5,9] This underscores an unmet clinical need to investigate (i) mechanisms integral to MES subtype and (ii) factors driving the molecular shift towards mesenchymal phenotype. More effective and targeted therapeutic strategies can then be potentially developed for MES GBM.

Single-cell profiling has also given insights into the intricacies of GBM microenvironment that significantly influence phenotypic switches in neoplastic cells and eventual response to therapy.[3,5,9–11] MES tumors, specifically, exhibit prominent myeloid infiltration[5,11] and through ligand-receptor interactions, myeloid populations have the capacity to trigger a mesenchymal transition in non-mesenchymal cell states.[3,9] The specific molecular players critical for the cross-talks remain inadequately elucidated and validated. Understanding these interactions is imperative for pinpointing therapeutic vulnerability for MES GBM.

To address these gaps in knowledge, we leverage Glioportal, our comprehensive repository of GBM patient tumors that comes along with the associated biofluids, cell lines, xenografts, and clinical and transcriptome data. Using cellular and xenograft models, we utilize Glioportal to better understand the multifariousness of MES GBM. Our transcriptomic analysis unravels the gene co-expression network and signaling pathways integral to MES subtype, as well as ligand-receptor pairs critical for interactions with myeloid populations and acquisition of mesenchymal phenotype.

Materials and Methods

Clinical Samples

Tumour tissues were obtained fresh at the time of surgical resection. Under the sterile condition, the tumor tissues were subdivided into small pieces, some of which were snap-frozen and stored at −150 °C for RNA extraction and sequencing. The leftover tissues were fixed in 4% paraformaldehyde for at least 24 hours at 4 °C. A portion of the fixed tissues was then dehydrated and embedded in paraffin, while the rest was soaked in 30% sucrose for at least 24 more hours at 4 °C, before quick freezing in optimal cutting temperature (OCT) medium. The frozen tissue blocks were stored at −80 °C. Clinical characteristics of Glioportal cohort are summarized in **Supplementary Table S1**.

Generation of glioma-propagating cells

The rest of the tumor pieces were processed to generate glioma-propagating cells (GPCs) following Gritti et al. with slight modifications.[12] Cells were tested for mycoplasma contamination and cultures were negative. All experiments were conducted with low passage GPCs for which we previously demonstrated maintenance of phenotypic, transcriptomic, and karyotypic features similar to the original primary tumors.[13]

Ethics Statement

De-identified GBM tumor specimens were obtained with informed consent from the National Neuroscience Institute Tissue Bank (application no. SBRSA2019/002). All animal experimental procedures were performed according to protocols approved by the Institutional Animal Care and Use Committee of Nanyang Technological University, Singapore (A24062).

Statistical Analysis

All bioinformatics data analyses were performed in R v4.3.1. Survival analysis was carried out using R/survival v3.5-7 and R/survminer v0.4.9.999. R/survivalAnalysis v0.3 was used to calculate the pairwise survival differences between PN, CL, and MES tumors of high simplicity scores (>0.99). *t*-test was used for cell state proportion scores, while non-parametric test was used for other comparisons, such as gene expression between groups. Data visualizations were created using the following R packages: ComplexHeatmap v2.16.0, ggplot2 v3.4.4, and ggforce v0.4.1. Experimental data are expressed as mean ± standard deviation (s.d.) of at least three independent experiments. Two-tailed student's *t*-test and Pearson correlation were used where appropriate. Kaplan-Meier survival curves were analyzed using log-rank test with Prism 5 (GraphPad Software). Statistical significance is indicated by *, *P*-value < .05; **, *P*-value < .01; ***, *P*-value < .001.

Detailed materials and methodology for bioinformatics analysis and in vitro, in vivo, and ex vivo experiments are available in **Supplementary Materials and Methods**.

Results

Glioportal for Translational Glioblastoma Research

Glioportal is a systematic biobank and transcriptomic resource for GBM, where tumor tissue specimens were acquired under Institutional Review Board (IRB) oversight with appropriate informed consent processes (**Figure 1A**). Unlike other tissue banks that practice complete anonymization,[14–20] Glioportal maintains ethical standards by employing a "Trusted Third Party" (TTP) approach to bridge communication between clinicians and scientists, thereby preserving critical patient information for research purposes. Following 2021 World Health Organization guidelines for GBM classification,[21] we collected primary tumors (PTs) with wild-type isocitrate dehydrogenase (IDHwt) (**Supplementary Table S1**). The biobank also covers patient-derived glioma-propagating cells (GPCs), mouse orthotopic xenografts (TXs), and associated biofluids (**Figure 1B**). Peripheral blood samples

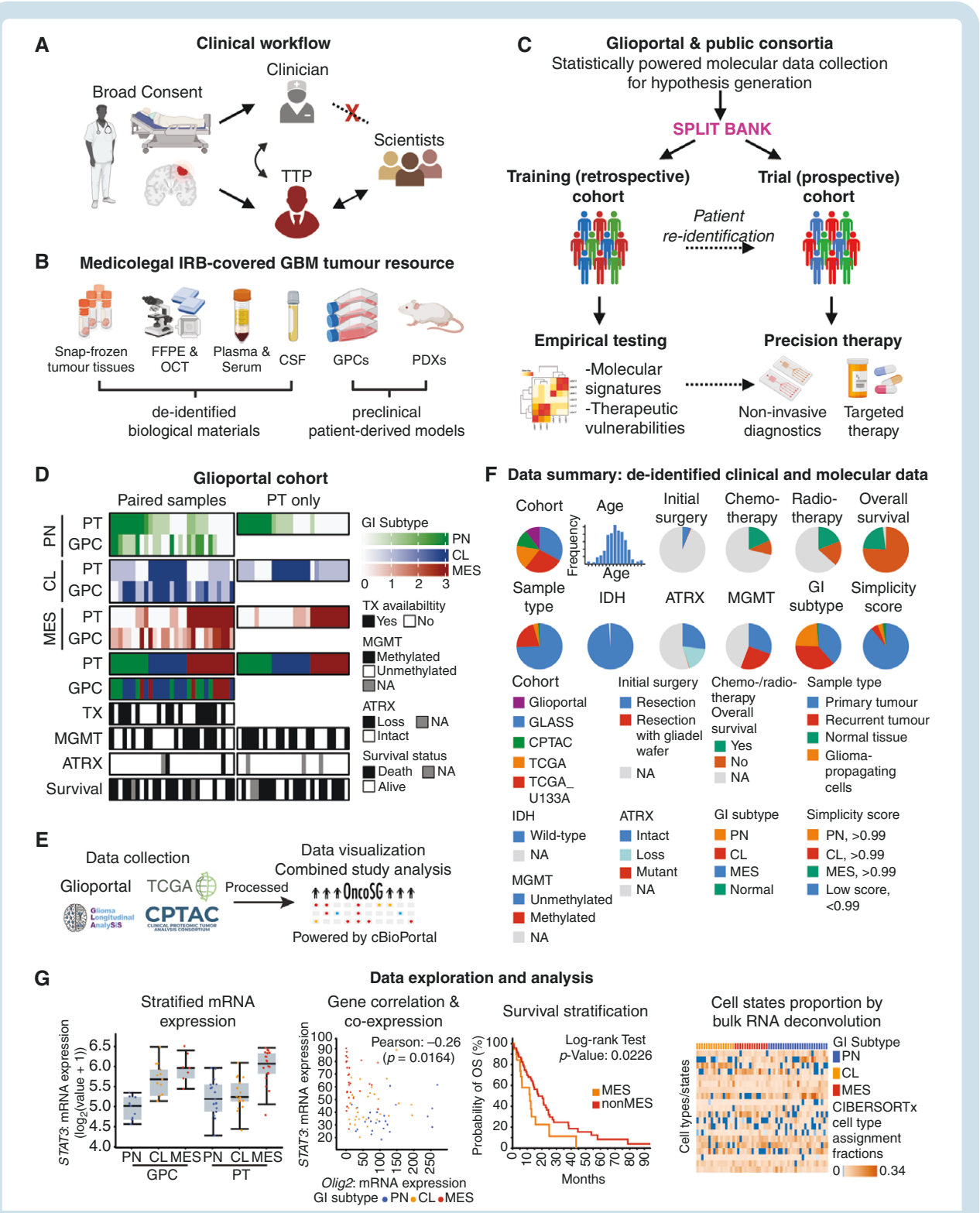

Figure 1. Glioportal is a dynamic and forward-looking glioblastoma tumor resource for precision therapy. **A.** Schematic of procurement of primary tumors (PTs) obtained with broad consent and de-identification of samples *via* a trusted third party (TTP). TTP bridged communications between clinicians and scientists for prospective patients' re-identification. **B.** PTs were immediately processed to generate glioma-propagating cells (GPCs), from which orthotopic patient-derived xenografts (PDXs) were established. Bulk RNA sequencing of snap-frozen PT and PDX tissues as well as GPCs was acquired. Leftover PT tissues were formalin-fixed for histopathology and immunohistochemistry. In parallel, patients' bloods were collected longitudinally, at pre- and post-surgery/therapy. De-identified clinical and molecular information were documented throughout the course of disease. **C.** In conjunction with publicly available consortia, Glioportal resource enables statistically robust hypothesis testing for prospective stratified trials and precision diagnostic and therapy designs. **D.** Stratification of Glioportal primary tumors based on glioma-intrinsic

(GI) transcriptomic subtype: proneural (PN), classical (CL), and mesenchymal (MES). All tumors have wild-type isocitrate dehydrogenase genes. "Paired samples" defines tumors with corresponding GPCs successfully generated; "PT only" defines tumors without GPCs. Each column represents a tumor case. Top three tracks correspond to the aggregate scores of the GI subtypes. The dominant subtype in each PT/GPC is shown in the fourth and fifth track, respectively. The availability of matched xenograft is indicated in the sixth track. ATRX, MGMT, and survival status are presented in the bottom three tracks. ATRX, alpha-thalassemia X-linked mental retardation; MGMT, O^6-methylguanine DNA methyltransferase. **E.** Schematic representation of GBM transcriptomic data collection and incorporation into the Singapore Oncology Data Portal (OncoSG). **F.** Data summary showcasing the distribution of clinical and molecular parameters of de-identified GBM samples. **G.** Data exploration and analysis enable users to query gene expression, correlation and co-expression, patient survival stratification, as well as cell state proportion based on bulk RNA sequencing deconvolution tools. Panels A-C were created in BioRender. Tang, C. (2025) https://BioRender.com/261btr9.

were longitudinally collected at pre- and post-surgery and -treatments. Our cohort taps into publicly available omics consortia, employing a split bank concept, where earlier patients' samples facilitate retrospective discovery, while recent patients can be re-identified for therapeutic target exploration in new clinical trials (**Figure 1C**).

From 55 PTs currently banked, we successfully generated 29 GPCs and established 15 TXs (**Figure 1D**). All tissues and cells were cryo-pulverized and subjected to bulk RNA sequencing, from which they were stratified following Wang's glioma-intrinsic (GI) transcriptomic classifier.[6] The de-identified molecular data and clinico-pathological features were housed in Glioportal at Singapore Oncology Data Portal, OncoSG (**Figure 1E and 1F**). Through this interactive resource (**Figure 1G**) https://src.gisapps.org/OncoS, users can analyze genes expression, correlation and co-expression, survival stratification, and cell states/types proportion by bulk RNA deconvolution in molecularly stratified GBM.

We observed a comparable number of PN ($n = 17/55$), CL, ($n = 18/55$), and MES ($n = 20/55$) GBM tumors in our cohort (**Figure 1D**). The majority of our GPCs (75%, $n = 22/29$) and TXs (53%, $n = 8/15$) retained their original tumours' transcriptomic profiles and were of PN and CL subtypes. Notably, 55% ($n = 6/11$) of our MES tumors lost their mesenchymal identity and transitioned to PN subtype in culture (**Supplementary Table S1**). Similarly, 67% ($n = 4/6$) of MES GPCs switched to PN/CL subtypes when stereotaxically implanted into immunodeficient NOD-SCID gamma (NSG) mice (**Supplementary Table S1 and Supplementary Figure S1A**). This suggests the prerequisite of the tumor microenvironment (TME)/stroma for maintaining mesenchymal transcriptional state.

To validate the clinical relevance of MES subtype, we analyzed survival outcomes in IDHwt tumors that have minimal transcriptional heterogeneity (high simplicity score of > 0.99) from our Glioportal cohort (**Supplementary Figure S1B**), combined with The Cancer Genome Atlas (TCGA)[4,6] and Clinical Proteomic Tumour Analysis Consortium (CPTAC; **Supplementary Figure S1C**).[5] Patients with MES-dominant tumors had significantly poorer overall survival relative to non-MES tumors (**Supplementary Figure S1D**; log-rank test, *P*-value = .023). This highlights the need to investigate the mechanisms driving mesenchymal aggressive phenotype and to discern potential therapeutic vulnerabilities for MES GBM.

STAT3 and NF-κB Pathways Govern Mesenchymal Glioblastoma

To uncover gene modules strongly associated with MES subtype, we conducted weighted gene co-expression network analysis (WGCNA) on our paired PTs and GPCs (**Figure 2A**, **Supplementary Figure S2 and Supplementary Table S2**). Over-representation analysis presented biological functions within each module. In line with previous studies,[6,22,23] MES subtype showed enrichment in module M1, with upregulation of mesenchymal transcriptional signature genes (**Supplementary Table S3**) and those implicated in TNF signaling *via* NF-κB pathway (**Figure 2B**). Another MES module M16 presented oxidative/glycolytic biological processes with expression of hypoxia programs previously reported in bulk and single-cell RNA sequencing datasets[7,24] (**Figure 2B**). Over-representation of both modules was maintained in MES GPCs (**Figure 2C and 2D**). In contrast, PN-specific modules correlated with neurodevelopmental functions (**Supplementary Figure S3A** and **Supplementary Table S4**), whilst CL-specific module overlapped with classical gene signature[6] (**Supplementary Figure S3B** and **Supplementary Table S5**).

To further validate the MES-intrinsic nature of modules M1 and M16, we assessed the expression changes of enriched signaling pathways (**Supplementary Figure S3C**) between (i) paired MES PTs and GPCs ("MES-MES"), and (ii) paired MES PTs and non-MES GPCs ("MES-nonMES") (**Supplementary Figure S3D-F**). "MES-nonMES" pairs showed significant downregulation of NF-κB, reactive oxygen species (ROS), and STAT3 signaling, whilst these pathways remained active in "MES-MES" pairs, indicating their importance for mesenchymal identity. Next, to predict master regulators in the gene hubs of MES modules M1 and M16, we employed a curated transcription factor (TF)-target interaction network.[25] Predictive analysis revealed key TFs governing module M1, amongst which were *STAT3*, *RUNX1*, *JUN* and *FOS*, as corroborated in previous studies[22,23,26–28] (**Figure 2E**). Similarly, *RelB*, and *FOSL1* were two leading regulons predicted to regulate module M16, linking them to NF-κB pathway and GBM plasticity and aggressiveness[22,29,30] (**Figure 2F**).

Therapy-induced shift to the MES subtype is common in recurrent disease,[9,31,32] potentially due to its permissive epigenetic landscape and altered DNA methylation patterns[33] as well as characteristic tumor-associated stroma.[3,6] Using initial-recurrent tumor pairs from Glioma Longitudinal Analysis Consortium (GLASS) cohort,[3] we assessed the relevance of MES modules M1 and M16 in tumors that underwent mesenchymal transitions upon recurrence. Feature reduction *via* a random forest-based method identified transcriptomic signatures to classify tumors by module enrichment. Initial non-MES tumors transitioning to MES subtype upon recurrence showed an increased frequency in the shift from "$M1^{low}$"/"$M1+M16^{low}$" to "$M1^{high}$"/"$M1+M16^{high}$" (**Figure 2G**; Fisher's Exact test,

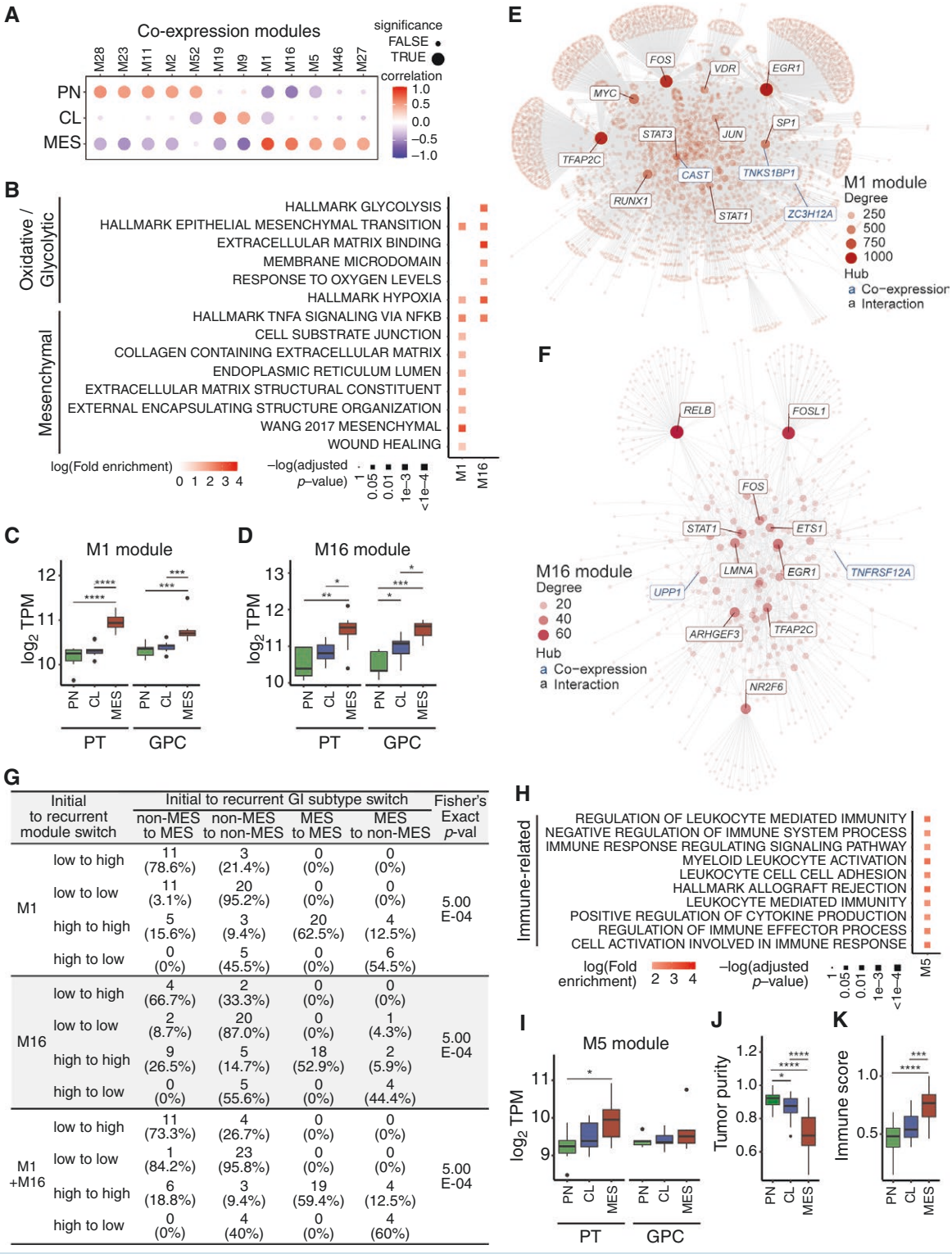

Initial to recurrent module switch		Initial to recurrent GI subtype switch: non-MES to MES	non-MES to non-MES	MES to MES	MES to non-MES	Fisher's Exact *p*-val
M1	low to high	11 (78.6%)	3 (21.4%)	0 (0%)	0 (0%)	5.00 E-04
	low to low	11 (3.1%)	20 (95.2%)	0 (0%)	0 (0%)	
	high to high	5 (15.6%)	3 (9.4%)	20 (62.5%)	4 (12.5%)	
	high to low	0 (0%)	5 (45.5%)	0 (0%)	6 (54.5%)	
M16	low to high	4 (66.7%)	2 (33.3%)	0 (0%)	0 (0%)	5.00 E-04
	low to low	2 (8.7%)	20 (87.0%)	0 (0%)	1 (4.3%)	
	high to high	9 (26.5%)	5 (14.7%)	18 (52.9%)	2 (5.9%)	
	high to low	0 (0%)	5 (55.6%)	0 (0%)	4 (44.4%)	
M1 +M16	low to high	11 (73.3%)	4 (26.7%)	0 (0%)	0 (0%)	5.00 E-04
	low to low	1 (84.2%)	23 (95.8%)	0 (0%)	0 (0%)	
	high to high	6 (18.8%)	3 (9.4%)	19 (59.4%)	4 (12.5%)	
	high to low	0 (0%)	4 (40%)	0 (0%)	4 (60%)	

Figure 2. Deciphering molecular drivers of mesenchymal glioblastoma. **A.** Dot plot depicting the correlation between module eigengenes and bulk transcriptional subtypes. **B.** Enriched terms in mesenchymal-associated co-expression modules, M1 and M16. **C & D.** Boxplot depicting the expression of genes in (C) M1, mesenchymal module, and (D) M16, oxidative/glycolytic module, in glioma-intrinsic (GI) transcriptomic subtype-stratified primary tumors (PTs) and glioma-propagating cells (GPCs). **E & F.** Gene networks of mesenchymal-associated modules (E) M1 and (F) M16. The topmost connected genes (hubs) reflect those initially present in the co-expression module and those inferred from the transcription factor (TF)-target interaction network. **G.** Contingency table showing correlation between mesenchymal-associated co-expression modules M1/M16 and GI subtype switch observed in GLASS initial cohort to recurrent GBM cohort. **H.** Enriched terms in M5, an immune-related mesenchymal module. **I.** Boxplot depicting the expression of genes in M5 module, in GI subtype-stratified PTs and GPCs. **J.** Tumour purity and **K.** immune scores in GI subtype-stratified PTs. Significance is denoted by asterisks: **P* < .05; ****P* < .001; *****P* < .0001.

P-value = 5 x 10^{-4}). The reverse was similarly observed in MES-to-non-MES switch, where there was an increased frequency in the shift from "$M1^{high}$/$M16^{high}$/M1+$M16^{high}$" to "$M1^{low}$/$M16^{low}$/M1+$M16^{low}$," highlighting the integral function of modules M1 and M16 in MES subtype.

Tumor Immune Microenvironment Regulates Mesenchymal Identity

In addition to modules M1 and M16, our network analysis also identified module M5 enriched in immune-related gene sets (**Figure 2H**, **Supplementary Table S3**), which was upregulated in MES tumors relative to PN and CL tumors (**Figure 2I**). In line with this observation, our MES tumors exhibited reduced tumor purity (**Figure 2J**), and elevated immune score (**Figure 2K**) compared to non-MES tumors. Unlike modules M1 and M16 which were enriched in both MES tumors and GPCs (**Figure 2C and 2D**), the enhanced expression of module M5 was not recapitulated in MES GPCs (**Figure 2I**), presumably due to the absence of interactions with tumor immune microenvironment as the cells were grown as spheroid cultures in vitro.

Interrogation of GBM TME, through brain tumor-specific microenvironment cell population counter RNA sequencing computational method, identifies three TME-specific classes: TME^{low}, $TME^{med,}$ and TME^{high}.[11] TME^{high} tumors exhibit high immune cell infiltration linked to immunosuppression markers. Assessment of GBM immunotherapy trial datasets showed that TME^{high} patients receiving neoadjuvant anti-PD-1 had significantly increased overall survival.[11] On account of the MES subtype predominating the TME^{high} class, we proceeded to evaluate whether M1 and M16 modules have implications in GBM TME profile and response to immunotherapy. Our Glioportal cohort analysis revealed a significant correlation between MES modules enrichment (M1 or M1 + M16) and TME^{high} subtype in recurrent cases (**Supplementary Table S6**; Fisher's Exact test, *P*-value = 5 x 10^{-4}). Conversely, we detected a prevalence in the shift from $M16^{high}$/M1 + $M16^{high}$ to $M16^{low}$/M1 + $M16^{low}$ phenotype in tumors that transition from TME^{high} to TME^{low} upon recurrence, suggesting a reciprocal relationship between mesenchymal-associated pathways and biological processes and TME.

Mesenchymal Glioblastoma Reveals Prominent Immune Cell Infiltration

We proceeded to comprehensively characterize the cellular components of GBM TME across subtypes. We leveraged cell-state signatures from GBmap[34] as a reference transcriptome for annotation of Neftel's malignant cell states[7] and non-neoplastic cell types, and applied CIBERSORTx,[34] a single-cell based deconvolution method, on our bulk RNA sequencing data (**Figure 3A**). Besides the predominating MES-like cell state, MES tumors exhibited a higher proportion of mural cells, smooth muscle cells, and pericytes of the vasculatures relative to non-MES tumors. MES tumors also showed prominent immune cell infiltration, particularly myeloid populations, which include monocytes, bone marrow-derived macrophages, and resident microglia. The enrichment of myeloid populations within MES tumors has been consistently observed by independent groups. Tumor-associated myeloid cells were reported to make up approximately 30-50% of the cell populations in GBM TME.[3,6,9,35–37] In contrast, PN tumors primarily constituted neural progenitor cell (NPC)-like and oligodendrocyte progenitor cell (OPC)-like malignant cell states, alongside resident oligodendrocyte, OPC and radial glia; whilst CL tumors featured astrocyte (AC)-like neoplastic cell state and resident astrocytes. Similar profiles were observed when CIBERSORTx deconvolution was carried out using combined cohorts of IDHwt cases from Glioportal, TCGA, and GLASS datasets (**Supplementary Figure S4A**, **S4B** and **Supplementary Table S7**, **S8**).

We further assessed quantitative associations between malignant cell states and TME using GBMdeconvoluteR[38] (**Figure 3B**, **Supplementary Figure S4C** and **Supplementary Table S9**). In agreement with CIBERSORTx deconvolution method, MES tumors showed significantly higher proportions of innate and adaptive immune populations relative to non-MES tumors. To validate this distinct immune cell enrichment, we examined in formalin-fixed and paraffin-embedded Glioportal PN and MES tumors, CD45 expression (a pan-leukocyte marker) and its spatial correlation with regard to CD44 and Olig2, a canonical mesenchymal and proneural marker, respectively (**Figure 3C**). Our findings were consistent with the single-cell-based deconvolution analysis, showing a significantly higher frequency of CD45-positive cells in MES compared to PN tumors (**Figure 3D**). The abundance of CD45-positive immune cells correlated significantly with mesenchymal CD44 marker (Pearson correlation coefficient $r = 0.821$, *P*-value = .012; **Figure 3E**) and showed a strong inverse relationship with proneural Olig2 marker (Pearson correlation coefficient $r = -0.788$, *P*-value = .02; **Figure 3F**).

Ligand–Receptor Pairs Mediate Cross-Talks Between Myeloid and Malignant Cell States

Transcriptome profiling of paired primary and recurrent GBM revealed significantly enhanced fractions of macrophages/microglia during non-MES to MES transition at recurrence.[3,6] Besides their prevalence in GBM ecosystem, there is mounting evidence demonstrating myeloid function in promoting GBM proliferation and migration and propositioning myeloid-targeted therapeutic strategies.[37,39] These findings affirm the pathological interplay between GBM neoplastic cells and myeloid populations and motivated us to interrogate potential ligand-receptor (LR) pairs that mediate communication between the two. We hypothesized that abrogating these ligand-receptor interactions could mitigate mesenchymal transition and therapy resistance upon recurrence. To test this, we examined upregulated targets, following the deconvolution of bulk RNA profiles, specific to myeloid and neoplastic cell states within primary tumors from Glioportal, TCGA, and GLASS GBM cohorts (**Figure 4A**).

From a repertoire of 1380 LR pairs identified in an earlier pan-cancer study,[40] we filtered for GBM-centric ligand- and receptor-encoding genes (**Supplementary Figure S5A**, **S5B** and **Supplementary Table S10**). By ranking the

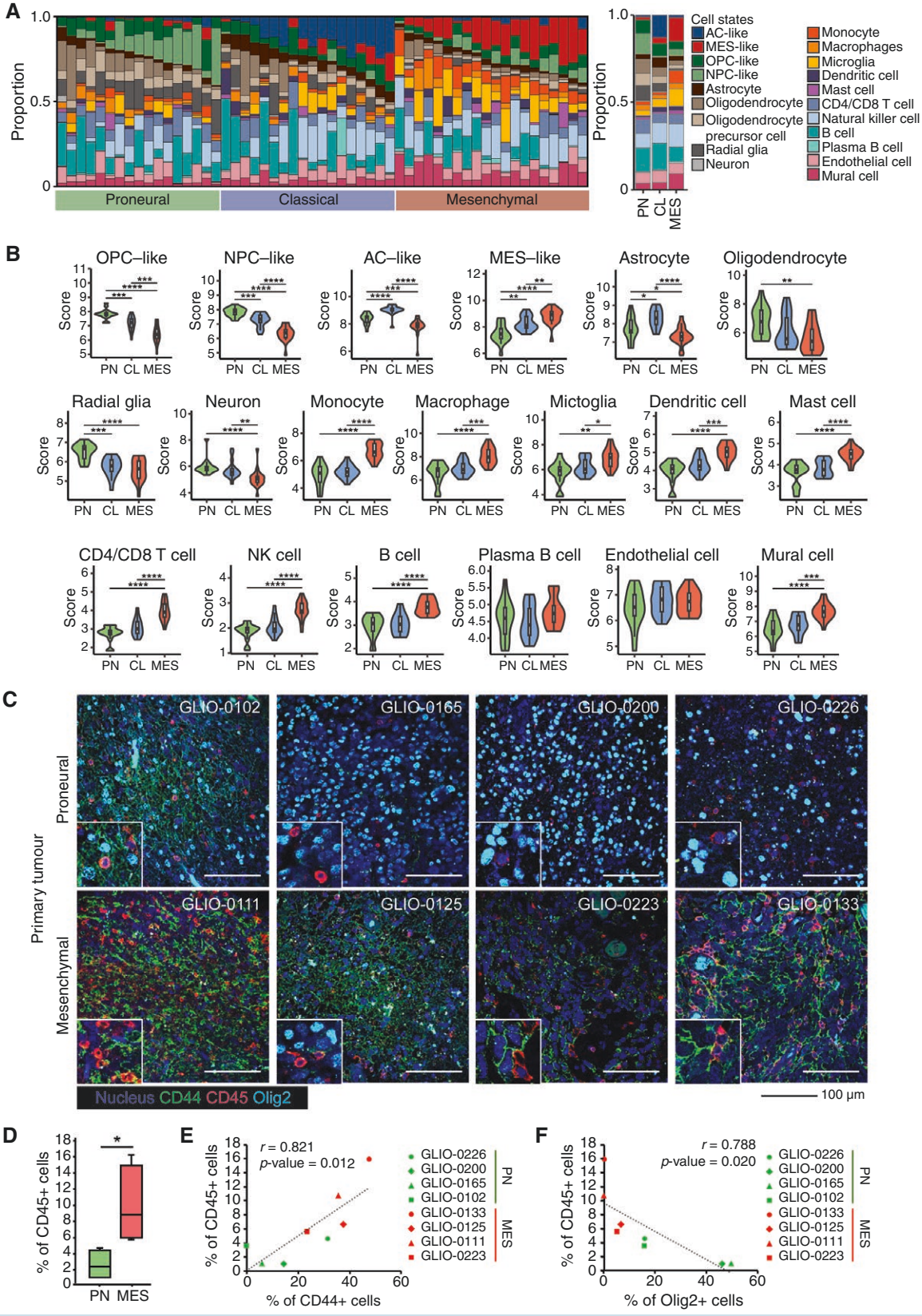

Figure 3. Mesenchymal glioblastoma displays prominent immune cell infiltration. **A.** Single-cell-based CIBERSORTx deconvolution analysis depicting cell state composition within each tumor (left, each column represents a tumor) and the average proportion (right). The tumors shown

are from Glioportal cohort stratified according to the glioma-intrinsic (GI) transcriptomic subtype. **B.** Violin plots showing the distribution of GBMdeconvoluteR cell state scores in GI subtype-stratified tumors. **C.** Representative immunofluorescent staining of CD45 (immune marker), CD44 (mesenchymal marker), and Olig2 (proneural marker) in formalin-fixed paraffin-embedded proneural versus mesenchymal primary tumors. **D.** Quantification of CD45-positive cells in proneural versus mesenchymal primary tumors ($n = 4$ primary tumors for each subtype). Scale bar: 100 µm. E **&** F. Correlation of CD45-positive and CD44- or Olig2-positive cells in each tumor. Pearson correlation coefficient (r) measures the strength of the relationship. Significance is denoted by asterisks: *$P < .05$; **$P < .01$; ***$P < .001$; ****$P < .0001$.

gene expression based on $\log_2$ fold change, we identified LR pairs predicted to regulate neoplastic cell plasticity towards mesenchymal phenotype, ie ligands that are highly expressed in myeloid cells, with corresponding receptors highly expressed in malignant cells (**Figure 4B**). Separately, we also identified LR pairs that potentially function in myeloid cell recruitment, i.e. ligands highly expressed in neoplastic cells, with corresponding receptors expressed in myeloid populations (**Supplementary Figure S6A-C**). Each ligand may bind to more than one receptor, alluding to extensive downstream effects executed by these interactions.

Focusing on LR pairs connected to mesenchymal shift, we shortlisted thirty myeloid-derived ligands, which include oncostatin M (*OSM)* and tumor necrosis factor (*TNF*) previously implicated in GBM mesenchymal transition[10,22,36,41]; secreted phosphoprotein 1 (*SPP1*) previously identified in *PTEN*-null GBM mouse model as the ligand involved in macrophage-glioma cross-talk that sustained tumor growth and progression[42] and proneural-to-mesenchymal transition.[43] Also, wingless-related integration site 5A (*WNT5A*) whose over-expression was reported to induce GBM stem cell differentiation into endothelial-like cells, thereby promoting GBM invasiveness and spread.[44,45]

To refine our list of ligands, we verified their expressions in myeloid populations, across five independent single-cell RNA sequencing datasets[7,46–49] (**Supplementary Table S11**; GSE131928,[7] syn22257780,[46] GSE157424,[47] GSE117891,[48] GSE148842,[49]), and confirmed the expression of the corresponding receptors in neoplastic cell states (**Figure 4C and Supplementary Figure S5C**). Combining top-expressing ligands from both bulk and single-cell RNA sequencing analysis, we proceeded to validate eleven ligands in vitro in terms of their capacity to induce mesenchymal transition, especially in proneural cells (**Figure 5A, top panel)**. Transforming growth factor-beta (*TGF-β*) known to induce mesenchymal transition in various solid tumors, including GBM,[50] was included in our ligands screening.

Ligand–Receptor Interaction Triggers Malignant Cell State Plasticity

We first estimated the proportion of malignant cell states within each of our GPCs by quantifying a metagene score using gene subsets from Neftel's non-MES-like and MES-like meta-module signatures. Samples were then ranked as predominantly PN or MES based on their metagene scores (**Supplementary Figure S7A**). The subtype identity of these GPCs was further validated *via* immunoblot, from which we observed MES GPCs showing higher expression of canonical MES markers STAT3 and CD44 relative to PN GPCs (**Supplementary Figure S7B**).

To measure mesenchymal shift in vitro, we employed a MES subtype-specific reporter[41] featuring synthetic locus control regions (sLCR) with 5–6 MES-specific cis-regulatory elements that drive the expression of mVenus reporter gene (pLVX-MGT-mVenus-puro, **Figure 5A**, bottom panel). The GPCs were lentivirally transduced with this reporter plasmid and treated with the candidate ligands. Flow cytometry quantitation of mVenus fluorescence revealed elevated expression upon exogenous addition of OSM, TNF, ciliary neurotrophic factor (CNTF), and TNF-related weak inducer of apoptosis (TWEAK/TNFSF12) (**Figure 5B, 5C**), thereby implicating these ligands in mesenchymal transition.

Multiple transcriptional factors, including *TAZ, STAT3, CEBP, OSMR, NF-κB,* and *HIF-1*α, are proposed as master regulators of the MES state.[51] In agreement, both STAT3 and NF-κB networks were implicated in our MES-intrinsic modules M1 and M16 (see **Figure 2E and 2F**). We therefore assessed the activation of these integral pathways upon ligand stimulation (**Figure 5D**). OSM, CNTF, TNF, and TWEAK treatments activated STAT3 signaling cascade, as indicated by its phosphorylation (Y705) status. In addition, TNF and TWEAK also activated the NF-κB pathway, as shown by p65 phosphorylation (S546). The importance of STAT3 and NF-κB activities in the mesenchymal shift was further corroborated using specific inhibitors (AZD1480 and BMS-345541, respectively) that could suppress the mesenchymal sLCR activation and hence the mVenus reporter gene expression (**Supplementary Figure S8A-F**). Notwithstanding other mesenchymal-associated pathways, we observed a general trend of PN GPCs being more receptive to ligands-induced STAT3 and NF-κB signaling activation, relative to MES GPCs. We speculate that PN GPCs have greater "potential" to undergo mesenchymal transition, as opposed to MES GPCs that are already mesenchymal, to begin with, as indicated by their higher basal STAT3 activity.

We found STAT3 and NF-κB pathways activation correlated with induced expression of mesenchymal-associated proteins (CD44, YKL-40, and TAZ) and suppressed expression of a proneural marker, Olig2 (**Supplementary Figure S7C and S7D**). In agreement, quantitative reverse transcription-PCR (qRT-PCR) analysis showed increased expression of a subset of Neftel's MES-like-associated genes, alongside a reduction in non-MES-like-related genes (**Figure 5E**). Together, these data further corroborated mVenus fluorescence tracking mesenchymal phenotype. Importantly, the cellular plasticity towards the mesenchymal state manifested in enhanced invasiveness, as demonstrated in PN GPCs treated with CNTF and TWEAK (**Supplementary Figure S8G-J**) as well as TNF (**Figure 6F and 6G**). Meanwhile, the effect of TGF-β on mesenchymal

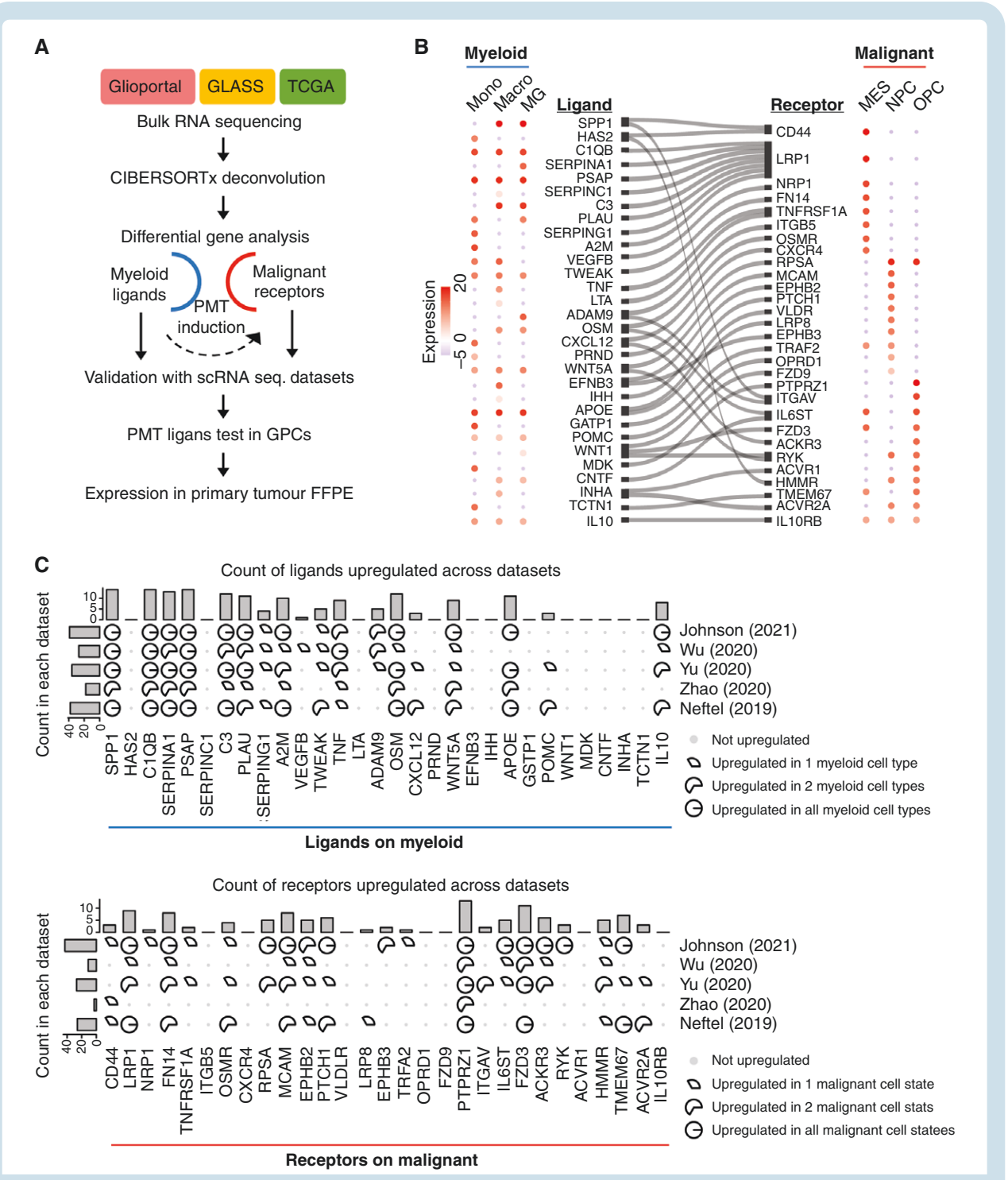

Figure 4. Ligand–receptors pairs implicated in myeloid and malignant cell cross-talks. **A.** Schematic workflow of ligand-receptor prioritization using cell state-specific gene expression profiles. **B.** Sankey flowchart depicting ligand-receptor interactions (Middle). The average ligands expression in myeloid populations (Left) and that of receptors in malignant cell states (Right) are shown. **C.** UpSet plot depicting counts of ligands and receptors upregulated in myeloid cell types (Top) and malignant cell states (Bottom), respectively, across five publicly available single-cell RNA sequencing datasets. Pie charts indicate the counts of the respective cell types/states in which the upregulation of expression was detected; for instance, one-third of a pie denotes enhanced expression in one out of three respective cell types/states (ie, monocytes/ macrophages/ microglia for myeloid populations or MES-like/ NPC-like/ OPC-like for malignant populations). Mono, monocytes; Macro, bone marrow-derived macrophages; MG, microglia.

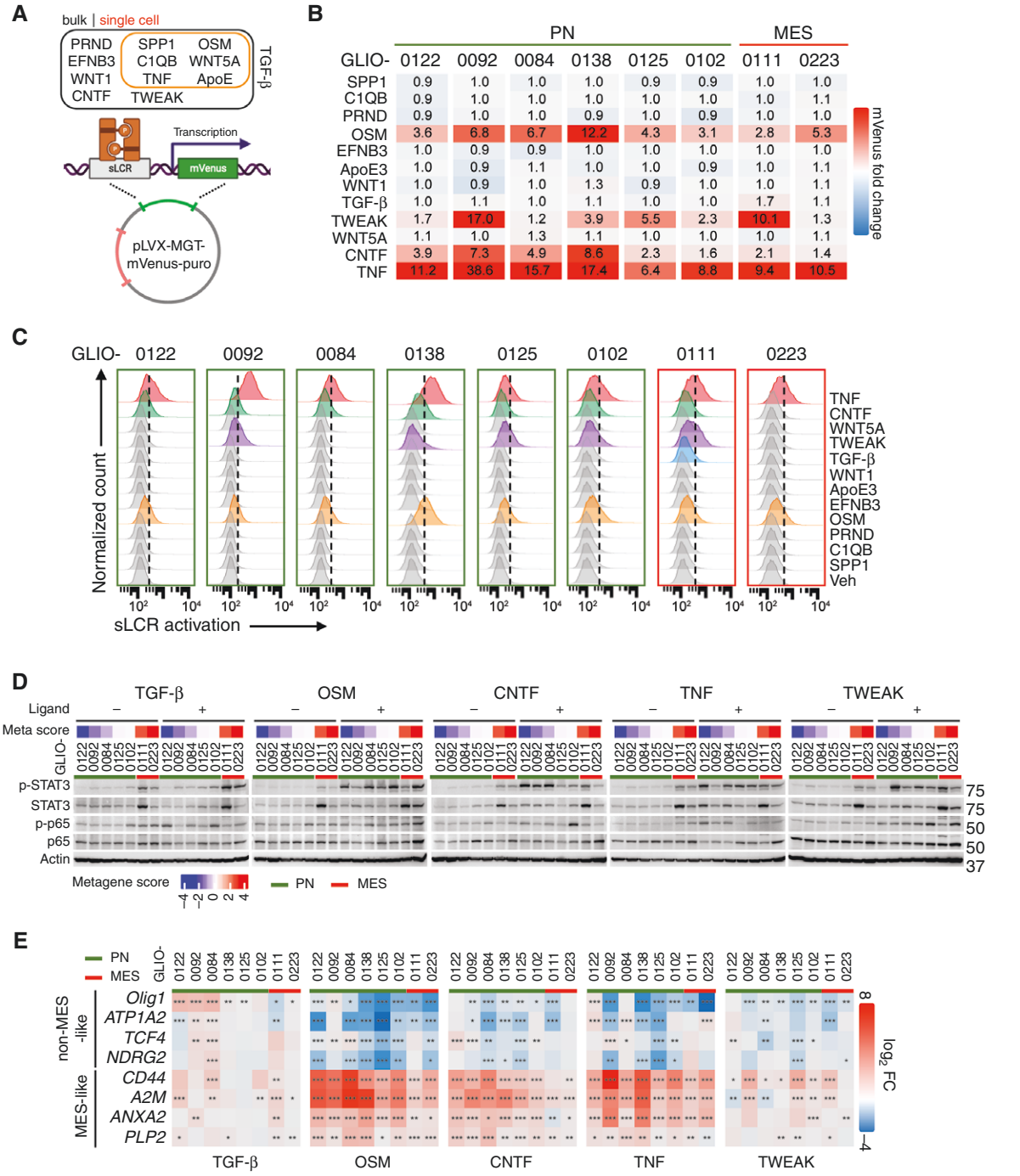

Figure 5. Predicted myeloid-derived ligands induce mesenchymal transition. **A.** (Top) Schematic of myeloid-derived ligands as predicted from bulk and single-cell RNA sequencing datasets. (Bottom) Mesenchymal subtype-specific lentiviral vector, carrying synthetic locus control region (sLCR) coupled with mVenus fluorescent reporter, which was utilized to screen for ligands that induced mesenchymal transition. The illustration was created with BioRenders.com. **B.** Heatmap of mVenus fluorescence fold change upon ligands treatment relative to vehicle control (average of $n = 3$ replicates). **C.** Representative mVenus fluorescence curve shift of (B) as determined by flow cytometry analysis. **D.** Representative immunoblots of STAT3 phosphorylation (Y705) and p65 phosphorylation (S536) upon 24-h ligands treatment. The GPCs were arranged according to metagene score, which defines the aggregate expression of Neftel's non-mesenchymal-like or mesenchymal-like gene signatures. Low metagene score represents higher activation of non-mesenchymal-like signature, high metagene score represents a predominant mesenchymal-like signature and white signifies activation of both signatures. **E.** Heatmap of Neftel's non-mesenchymal-like and mesenchymal-like genes expression upon 24-hour ligand treatment (average of $n = 3$ replicates). Significance is denoted by asterisks: $^{*}P < .05$; $^{**}P < .01$; $^{***}P < .001$, two-tailed Student's *t*-test. Green and red lines indicate proneural and mesenchymal subtype, respectively.

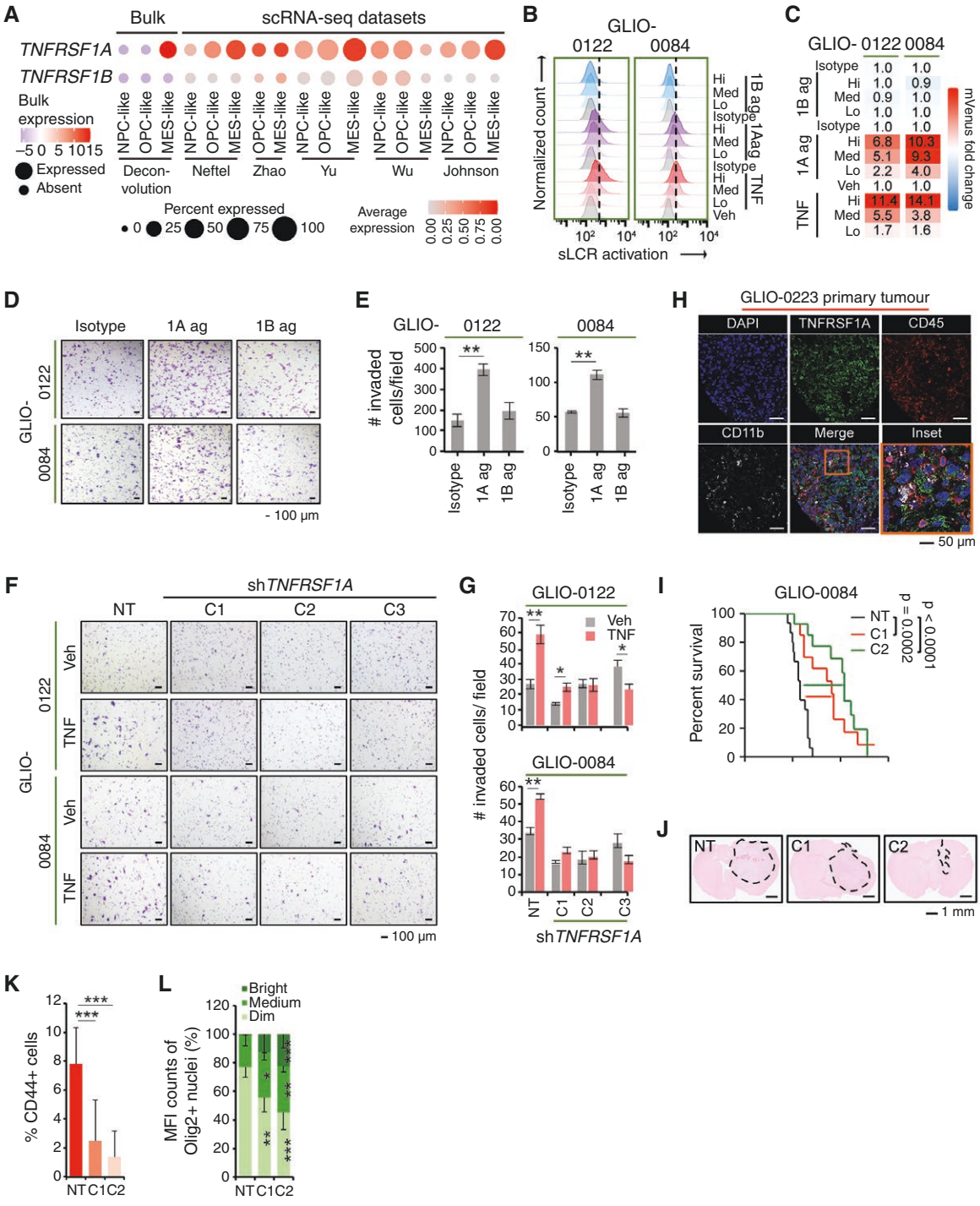

Figure 6. TNF-TNFRSF1A ligand-receptor pair promotes mesenchymal transition and confers invasive trait. **A.** *TNFRSF1A* and *TNFRSF1B* expression in malignant cell states based on deconvoluted sample-level cell state-specific gene expression and publicly available single-cell RNA sequencing datasets. **B.** Representative mVenus fluorescence curve shift in proneural cells, GLIO-0122 and -0084, upon 24-h agonistic antibody or TNF ligand treatment. **C.** Heatmap of mVenus fluorescence fold change upon 24-h agonistic antibody or TNF ligand treatment relative to respective isotype/ vehicle control (average of $n = 3$ replicates). **D.** Representative images of invaded cells upon 24-hour agonistic antibody treatment. Scale bar: 100 µm. **E.** Quantification of the number of invaded cells. **F.** Representative images of invaded cells upon *TNFRSF1A* silencing (three short hairpin RNA (shRNA) clones, C1, C2 and C3). Scale bar: 100 µm. **G.** Quantification of the number of invaded cells. **H.** Representative immunofluorescent co-staining of TNFRSF1A, CD45 (pan-leukocyte), and CD11b (pan-myeloid) in formalin-fixed paraffin-embedded GLIO-0223 mesenchymal primary tumor. Scale bar: 50 µm. **I.** Kaplan-Meier survival plot comparing tumors bearing non-targeting (NT) and two *TNFRSF1A*-targeting shRNA clones, C1 and C2 ($n = 15$ mice per group). **J.** Representative hematoxylin and eosin staining of the orthotopic tumors. Scale bar, 1 mm. **K.**

Quantification of CD44-positive GBM cells within the tumors. Error bars represent the standard deviation of six fields of view. **L.** Quantification of Olig2-positive GBM cells stratified into bright, medium, and dim mean fluorescent intensity (MFI) within each nucleus. Error bars represent the standard deviation of at least six fields of view. 1A ag, TNFRSF1A agonistic antibody; 1B ag, TNFRSF1B agonistic antibody; sLCR, synthetic locus control region. Significance is denoted by asterisks: *$P < .05$; **$P < .01$; ***$P < .001$, two-tailed Student's *t*-test. Data are mean ± s.d.

program activation was rather subdued (**Figure 5B, 5C**). Phosphorylation of Smad2 (S465/467) upon TGF-β addition indicated binding to its receptor (**Supplementary Figure S7C and S7D**), but with a change in the transcriptomic profile that paled in comparison with the rest of the ligands (**Figure 5E**).

TNF Binding to TNFRSF1A Confers Mesenchymal Phenotype and Invasiveness

With consistent induction of MES program across all tested GPCs, we zoomed into TNF function in the mesenchymal shift. TNF has two well-known receptors, TNFRSF1A and TNFRSF1B.[52] Deconvoluted bulk transcriptome data showed *TNFRSF1A* expression in MES-like cell state regardless of tumor subtypes, whilst *TNFRSF1B* was entirely absent (**Figure 6A**). Five independent public single-cell RNA sequencing datasets[7,46–49] further corroborated the differential *TNFRSF1A* and *TNFRSF1B* expressions, where *TNFRSF1A* expression was predominantly detected in MES-like neoplastic cell state, but also evident in NPC- and OPC-like states. Meanwhile, *TNFRSF1B* was detectable across all states, albeit at a generally much lower coverage and expression level relative to *TNFRSF1A*. At the protein level, both PN and MES GPCs in our cohort expressed TNFRSF1A, while only those with high metagene score (ie, possessed relatively more mesenchymal traits) expressed TNFRSF1B (**Supplementary Figure S9A**).

To further substantiate TNFRSF1A as the receptor responsible for mesenchymal transition, we treated GPCs that have the lowest metagene score (ie, possessed relatively more proneural traits) with agonistic antibodies targeting either receptor. Only TNFRSF1A engagement phenocopied TNF-induced mesenchymal sLCR activation (**Figure 6B and Supplementary Figure S9B**) and mVenus reporter gene expression (**Figure 6C and Supplementary Figure S9C**). Similar findings were replicated in *TNFRSF1B*-expressing GPCs (GLIO-0125 and -0223) (**Supplementary Figure S9B and S9C**). This was accompanied by concurrent activation of STAT3 and NF-κB pathways (**Supplementary Figure S9D**) and upregulation of mesenchymal-associated genes (*CD44, YKL-40, Vim,* and *TAZ*) (**Supplementary Figure S9E**). TNF is a well-known pro-inflammatory cytokine with pleiotropic effects including tumor growth and invasion. Using Matrigel® invasion chamber, we showed that agonistic antibody treatment targeting TNFRSF1A, but not TNFRSF1B, enhanced cell invasion towards chemoattractant (2% fetal bovine serum in bottom chamber, **Figure 6D and 6E**).

We continued verifying the TNFRSF1A function in triggering plasticity towards MES program by two approaches. Neutralizing antibody targeting TNFRSF1A, but not TNFRSF1B, significantly diminished TNF-induced upregulation of mesenchymal-associated genes in both PN GPCs (GLIO-0122, -0092 and -0084) and *TNFRSF1B*-expressing GPCs (GLIO-0125 and -0223; **Supplementary Figure S9F**). In addition, three independent short hairpin RNA (shRNA) knockdown clones of *TNFRSF1A* (C1-3) suppressed TNF-induced phosphorylation of STAT3 and p65, and upregulation of mesenchymal markers (**Supplementary Figure S9G**). Importantly, *TNFRSF1A* depletion also significantly reduced TNF-induced invasiveness (**Figure 6F and 6G**). Utilizing three corresponding formalin-fixed paraffin-embedded tumors, we observed proximity of TNFRSF1A-expressing cells with CD11b-positive myeloid populations (**Figure 6H and Supplementary Figure S10A**). Notwithstanding other LR pairs implicated in neoplastic cell state plasticity, these results established the function of TNF-TNFRSF1A interaction in mediating mesenchymal transformation.

Loss of *TNFRSF1A* Improves Mouse Survival

To assess whether TNF-TNFRSF1A function in mesenchymal transition has potential implications on disease prognosis, we carried out a proof-of-concept animal experiment. We lentivirally transduced our PN cell, GLIO-0084, with non-targeting (NT) shRNA control and two independent knockdown clones of *TNFRSF1A* (C1 and C2). We stereotaxically co-implanted GLIO-0084 with THP-1, a human monocytic cell line, to compensate for defective macrophage function in an immunodeficient NSG mouse strain. Similar preclinical models using either THP-1 or U937, another human monocytic cell line, have been previously employed by independent groups investigating the mechanisms of tumor-associated myeloid populations in promoting GBM progression.[53–58]

In vitro, exposure to a conditioned medium from THP-1-derived macrophages (**Supplementary Figure S10B and C**) strongly induced mesenchymal marker expression, CD44, and suppressed that of proneural Olig2 in our proneural cells. These effects were dampened by *TNFRSF1A* silencing (**Supplementary Figure S10D**). Functionally, loss of *TNFRSF1A* diminished cellular invasiveness stimulated by the conditioned medium (**Supplementary Figure S10E**). In agreement, we found mice bearing orthotopic *TNFRSF1A*-knockdown tumors had a significantly improved probability of survival (**Figure 6I**) and smaller tumor sizes (**Figure 6J**) relative to control tumors. NT mice had a median survival of 57 days in contrast to C1 and C2 mice with median survival of 90 and 103 days, respectively. The better prognosis correlated with a decreased frequency of GBM cells expressing CD44 and an increased frequency of those with enhanced nuclear Olig2 expression (**Figure 6K, 6L and Supplementary Figure S10F and G**). These results further affirmed TNF-TNFRSF1A function in the acquisition of mesenchymal phenotype and substantiated prognostic implications of mesenchymal transition.

Discussion

GBM remains one of the most challenging primary adult malignant brain tumors to treat, where chemotherapy is still limited to TMZ and treatment decisions have not yet fully adapted to inter- and intramolecular heterogeneity. Large GBM consortiums, like GLASS and CPTAC, have revealed the granularity of GBM complexity, providing insights into phenotypic plasticity occurring in neoplastic cells and characteristics of GBM tumor ecosystem that very much regulates the malignant cell state plasticity as the disease progresses.[3,5] Despite the wealth of data, the challenge remains to translate these new paradigms into functional, therapeutic, and curative outcomes. While tackling the MES GBM subtype has potential clinical benefits,[9,31,59] targeted therapeutic modalities remain scarce. In this study, we introduce Glioportal, the first GBM biobank in Asia that is aligned with the 2021 World Health Organization guidelines[21] and offers a comprehensive platform that integrates molecular data with therapeutic applications, ultimately aiming to improve treatment outcomes for this challenging disease.

Glioportal operates on a "split bank concept" where earlier patients' materials support discovery and preclinical research, while more recent patients can be re-identified for clinical trials. One example is the STAT3 gene signature that we previously established to stratify retrospective GBM patients into STAT3-high and STAT3-low cohorts.[26] This signature is more accurate than STAT3 phosphorylation status alone for predicting GBM patients' response to STAT3-targeting interventions.[26] Orthotopic xenografts derived from these GPCs facilitated preclinical validation of STAT3 inhibitor efficacy and combinatorial therapeutic strategies in both STAT3-high and -low cohorts. These findings formed the foundation of our EZ-READ (enzyme ZIF-8 complexes for regenerative and catalytic digital detection of RNA) nanosensor platform that accurately profiles circulating RNAs for blood-based GBM diagnosis and molecular subtyping.[60] We are currently fine-tuning the nanosensor platform to enable non-invasive stratification of GBM patients for STAT3-targeted clinical trials.

Separately, we identified p38 MAPK as a therapeutic vulnerability and druggable kinase for the MES subtype.[61] We demonstrated the synergy between TMZ and p38 MAPK inhibition in extending overall survival in orthotopic MES xenografts. Our findings advocate the use of targeted combination therapies to tackle the therapeutic-resistant subpopulation of the tumor. Also, we recently shared our findings on the functional dichotomy of enhancer of zeste homolog 2 (EZH2) in ROS-stratified GBM, where ROS(+) tumors are dominated by MES GBM subtype. ROS(+) GPCs and TX show dependency on EZH2 co-interaction with RelB and RelA to drive constitutive activation of non-canonical NF-κB2 signaling, rendering it resistant to TMZ.[62] Altogether, Glioportal resource captures the intra- and inter-patient variability and bridge the gap between molecular stratification and functional therapeutic outcomes.

Here, we leveraged the Glioportal biobank and utilized our paired PTs and GPCs to uncover "transcriptional addiction" within the MES GBM subtype. We found two intrinsic modules M1 and M16 that have implications in TME architecture and plasticity towards mesenchymal phenotype upon recurrence (**Figure 2G** and **Supplementary Table S6**). In addition, we found enrichment of immune-related module M5 indicating the significance of stromal elements in MES GBM. This was further corroborated by the loss of mesenchymal identity in MES tumor-derived GPCs and TXs (**Figure 2I** and **Supplementary Figure S1A**). Previous studies have established that the propagation of tumor cells over serial passages can lead to clonal expansion that fails to sustain intratumoral heterogeneity.[63] Moreover, the absence of tissue architecture and cellular constituents of TME exacerbate transcriptomic divergence from the original tumors.[59] Not surprisingly, the transcriptomic profiles of most GPCs derived from MES tumors and TXs established from MES GPCs switched to non-MES subtypes. We nonetheless took advantage of this phenotypic plasticity to screen for myeloid-derived ligands that have the capacity to induce mesenchymal transition (**Figure 5**).

Using mesenchymal-specific synthetic genetic tracing reporter,[41] we confirmed mesenchymal program activation induced by OSM[3,10,64] and TNF.[22,36,41] We also identified two ligands—CNTF and TWEAK (TNFSF12)—that are yet to be implicated in mesenchymal shift in GBM. CNTF, a neuropoietic cytokine, regulates astroglial differentiation in neural stem cells.[65] Alongside OSM, leukemia inhibitory factor (LIF) and interleukin 6 (IL 6), CNTF forms a cytokine family that shares structural similarities with one another and binds to gp130 receptor component thereby initiating JAK/STAT signaling cascade.[66] Consistent with the previous report,[41] we indeed observed mesenchymal sLCR activation upon LIF stimulation (data not shown).

On the other hand, TWEAK (TNFSF12), a TNF ligand family cytokine,[67,68] binds to Fn14 (TNFRSF12A) receptor and activates both canonical and non-canonical NF-κB pathways.[69,70] Elevated expression of *Fn14* receptor was previously detected in recurrent GBM and TMZ-resistant patient-derived xenografts.[71] *Fn14* over-expression in transgenic PN mouse models led to significantly reduced survival, accompanied by transformation into highly invasive, necrotic, and immune cell-rich tumors.[72] More interestingly, recent development of anti-Fn14 bispecific T-cell engager (BiTE) and Fn14-specific chimeric antigen receptor T (CAR-T)/IL-15 cells have shown promising antitumor activity in vitro, with significant tumor regression in xenograft models.[73] Thus, CNTF- and TWEAK-mediated induction of mesenchymal program through STAT3 and NF-κB signaling nodes highlights the prognostic values of M1 and M16 MES modules identified.

Notwithstanding other LR pairs implicated in neoplastic cell state plasticity, our ligand screening demonstrated TNF as a robust trigger for mesenchymal transition through specific engagement of TNFRSF1A (**Figure 6** and **Supplementary Figure S9**). Intriguingly, high *TNFRSF1A* expression was detected in malignant cells despite its well-established pro-apoptosis effects,[74] whilst the expression of *TNFRSF1B*, known for its proliferative function, paled in comparison (**Figure 6A**). TNFRSF1A and TNFRSF1B were shown to jointly modulate the activity of primed neural stem cells (NSCs) during systemic inflammation, where TNF binding to TNFRSF1B induces NSCs to engage the cell cycle and TNFRSF1A stimulation pulls the NSCs back to deep quiescence.[75] This functional divergence

arises from distinct intracellular domains of both receptors. Despite the presence of a cytoplasmic death domain, TNFRSF1A can activate NF-κB and other pro-survival pathways depending on the downstream formation of adaptor protein complexes. For instance, the TRAF2-cIAP1 complex recruitment to the TNFRSF1A death domain confers TNF pro-tumorigenic function, whilst its ablation redirects interaction with the RIPK1-caspase 8 complex, favoring cancer cell death.[76]

Our experimental data compellingly demonstrate TNFRSF1A function in mesenchymal transformation, whereas TNFRSF1B's role remains to be elucidated. Cooperation between the two receptors in balancing pro- and anti-tumorigenic effects of TNF is conceivable as demonstrated in the neuroblastoma co-culture model, where membrane-bound TNF expressed on cancer cells bind to monocytic TNFRSF1B thereby stimulating soluble TNF production that in turn binds to TNFRSF1A on the neoplastic cells and triggers pro-survival NF-κB signaling.[77] Future exploration of the interplay between TNFRSF1A and TNFRSF1B in the MES GBM subtype is warranted.

In summary, we communicated our endeavor to establish Glioportal as a resource platform for basic and translational GBM research. The growing number of biobanks alike illustrates its value in advancing precision therapy for GBM, especially with the rapid rise and availability of multi-omics capabilities and wealth of data that require rigorous validation using reliable preclinical models and well-curated molecular data.[14,15,17–20,78–80] Here, we tapped into Glioportal to identify both cell-intrinsic and -extrinsic factors critical for MES GBM. Ligand-receptor pairs function as conduits for mesenchymal phenotypic switch induced by the tumor immune microenvironment. They present potential therapeutic vulnerabilities for clinical scenarios when a GBM tumor recurs along a non-MES to MES axis. Their capacity to regulate neoplastic cell plasticity merits the pursuit of treatment strategies targeting cancer cell interactions with TME components.

Supplementary material

Supplementary material is available online at *Neuro-Oncology* (https://academic.oup.com/neuro-oncology).

Keywords

glioblastoma tumor resource | mesenchymal transition | cellular plasticity | ligand–receptor interaction | tumor necrosis factor

Acknowledgments

The computational work was partially performed using resources from the National Supercomputing Centre Singapore and Computational Health Research and Optimisation for Medical Advancements (CHROMA). We would like to thank Professor Ong Sin Tiong for THP-1 cell line and Mr Ron Weng Yee Loh for discussions concerning the work presented in this manuscript.The graphical abstract of this manuscript was created in BioRender. Tang, C. (2025) https://BioRender.com/f9av6r2.

Author Contributions

Conceptualization: Q.Y.P., C.T., P.T., B.T.A. Methodology: Q.Y.P., W.N., L.W.H.K., Y.K.C., S.W.L., N.L.S., S.R., J.L., H.S., N.S.T., S.Y., A.M.J.S., C.T., P.T., B.T.A. Validation: Q.Y.P., W.N., L.W.H.K., Y.K.C., S.W.L., C.T., B.T.A. Investigation: Q.Y.P., W.N., L.W.H.K., Y.K.C., S.W.L., C.T., B.T.A. Resources: X.L., S.Y.L.A., J.R.-X.K., K.-R.W., D.C.Y.L., M.C., W.W.B.G., S.Y., A.M.J.S., C.T., P.T., B.T.A. Data curation: Q.Y.P., N.L.S., S.R., A.M.J.S.

Writing – original draft preparation: Q.Y.P., W.N., L.W.H.K. Writing – review and editing: Q.Y.P., W.N., L.W.H.K., Y.K.C., S.W.L., J.L., W.W.B.G., N.S.T., C.T., P.T., B.T.A. Visualization: Q.Y.P., W.N., L.W.H.K., Y.K.C., S.W.L., C.T., B.T.A. Supervision: C.T., P.T., B.T.A. Funding acquisition: C.T., B.T.A.

Conflict of interest statement. The authors declare no conflict of interest.

Funding

This research is supported by the Singapore Ministry of Health's National Medical Research Council under its Translational and Clinical Research Flagship Programme-Tier 1 (NMRC/TCR/016-NNI/2016) and the National Research Foundation Singapore under its Open Fund-Large Collaborative Grant (OF-LCG) – Tier 1 (MOH-000541-00) awarded to B.T.A.; the Health Professional Investigator Program (HPI-2022-2834) from British Columbia's Michael Smith Health Research awarded to S.Y. The organizations that provided the grants had no role in study design, data collection and analysis, decision to publish or preparation of the manuscript.

Data Availability

The data supporting the results in this study are available within the paper and its Supplementary Information. To protect patient privacy, the Ministry of Health (MOH) of Singapore has imposed regulations on all healthcare institutions that no raw patient sequencing data can be stationed outside of the hospital network due to potential risks of re-identifying patients. Informed patient consent was obtained in accordance with these regulations, meaning that consent to data deposition in a public repository was not provided. Raw sequencing data that support the findings of this study are therefore available upon request due to patient privacy protection. Request for raw data access should be directed to Beng Ti Ang (ang.beng.ti@singhealth.com.sg). Review of the request will be completed within two months. Upon request approval by the National Neuroscience Institute Tissue Bank,

data will be accessible for research use only. The processed RNA sequencing data can be accessed from OncoSG under the study: Glioportal. Access to Glioportal at OncoSG should be directed to Qing You Pang (eddy_pq_you@nni.com.sg).

Affiliations

Neuro-Oncology Research Laboratory, Department of Research, National Neuroscience Institute, Singapore 308433, Singapore (Q.Y.P., W.N., L.W.H.K., Y.K.C., S.W.L., C.T., B.T.A.); Laboratory of Computational Cancer Genomics, Genome Institute of Singapore, Agency for Science, Technology and Research (A*STAR), Singapore 138672, Singapore (N.L.S., S.R., A.M.J.S.); Laboratory of Single-Cell Spatial Neuromics, Genome Institute of Singapore, Agency for Science, Technology and Research (A*STAR), Singapore 138672, Singapore (J.L.); Department of Neurology, National Neuroscience Institute, Singapore 308433, Singapore (X.L.); Department of Neurosurgery, National Neuroscience Institute, Singapore 308433, Singapore (S.Y.L.A., J.R.-X.K., K.-R.W., D.C.Y.L., B.T.A.); SingHealth Duke-NUS Neuroscience Academic Clinical Programme, Duke-National University of Singapore Medical School, Singapore 169857, Singapore (S.Y.L.A., J.R.-X.K., K.-R.W., D.C.Y.L., B.T.A.); Department of Mathematical Sciences, Chalmers University of Technology, University of Gothenburg, SE-412 96 Gothenburg, Sweden (M.C.); Lee Kong Chian School of Medicine, Nanyang Technological University, Singapore 308232, Singapore (W.W.B.G., N.S.T.); School of Biological Sciences, Nanyang Technological University, Singapore 637551, Singapore (W.W.B.G., N.S.T.); Center for Biomedical Informatics, Nanyang Technological University, Singapore 308232, Singapore (W.W.B.G.); Center of AI in Medicine, Nanyang Technological University, Singapore 308232, Singapore (W.W.B.G.); Division of Neurology, Department of Brain Sciences, Faculty of Medicine, Imperial College London SW7 2AZ, UK (W.W.B.G.); Institute for Health Innovation & Technology, National University of Singapore, Singapore 117599, Singapore (H.S.); Department of Biomedical Engineering, College of Design and Engineering, National University of Singapore, Singapore 117575, Singapore (H.S.); Institute of Molecular and Cell Biology, Agency for Science, Technology and Research (A*STAR), Singapore 138673, Singapore (H.S.); Department of Surgery, Yong Loo Lin School of Medicine, National University of Singapore, Singapore 117597 (H.S.); Department of Pathology & Laboratory Medicine, University of British Columbia, Vancouver, BC, Canada V6T 2B5 (S.Y.); Cancer and Stem Cell Biology Program, Duke-National University of Singapore Medical School, Singapore 169857, Singapore (C.T., P.T.); Genome Institute of Singapore, Agency for Science, Technology and Research (A*STAR), Singapore 138672, Singapore (P.T.); Cancer Science Institute of Singapore, National University of Singapore, Singapore 117599, Singapore (P.T.); Department of Physiology, Yong Loo Lin School of Medicine, National University of Singapore, Singapore 117593, Singapore (P.T.)

References

1. Ostrom QT, Price M, Neff C, et al. CBTRUS statistical report: primary brain and other central nervous system tumors diagnosed in the United States in 2016-2020. *Neuro Oncol*. 2023;25(12 Suppl 2):iv1–iv99.
2. Stupp R, Mason WP, van den Bent MJ, et al; European Organisation for Research and Treatment of Cancer Brain Tumor and Radiotherapy Groups. Radiotherapy plus concomitant and adjuvant temozolomide for glioblastoma. *N Engl J Med*. 2005;352(10):987–996.
3. Varn FS, Johnson KC, Martinek J, et al; GLASS Consortium. Glioma progression is shaped by genetic evolution and microenvironment interactions. *Cell*. 2022;185(12):2184–2199.e16.
4. Verhaak RG, Hoadley KA, Purdom E, et al; Cancer Genome Atlas Research Network. Integrated genomic analysis identifies clinically relevant subtypes of glioblastoma characterized by abnormalities in PDGFRA, IDH1, EGFR, and NF1. *Cancer Cell*. 2010;17(1):98–110.
5. Wang LB, Karpova A, Gritsenko MA, et al; Clinical Proteomic Tumor Analysis Consortium. Proteogenomic and metabolomic characterization of human glioblastoma. *Cancer Cell*. 2021;39(4):509–528.e20.
6. Wang Q, Hu B, Hu X, et al. Tumor evolution of glioma-intrinsic gene expression subtypes associates with immunological changes in the microenvironment. *Cancer Cell*. 2017;32(1):42–56.e6.
7. Neftel C, Laffy J, Filbin MG, et al. An integrative model of cellular states, plasticity, and genetics for Glioblastoma. *Cell*. 2019;178(4):835–849.e21.
8. Patel AP, Tirosh I, Trombetta JJ, et al. Single-cell RNA-seq highlights intratumoral heterogeneity in primary glioblastoma. *Science*. 2014;344(6190):1396–1401.
9. Wang L, Jung J, Babikir H, et al. A single-cell atlas of glioblastoma evolution under therapy reveals cell-intrinsic and cell-extrinsic therapeutic targets. *Nat Cancer*. 2022;3(12):1534–1552.
10. Hara T, Chanoch-Myers R, Mathewson ND, et al. Interactions between cancer cells and immune cells drive transitions to mesenchymal-like states in glioblastoma. *Cancer Cell*. 2021;39(6):779–792.e11.
11. White K, Connor K, Meylan M, et al. Identification, validation and biological characterisation of novel glioblastoma tumour microenvironment subtypes: implications for precision immunotherapy. *Ann Oncol*. 2023;34(3):300–314.
12. Gritti A, Parati EA, Cova L, et al. Multipotential stem cells from the adult mouse brain proliferate and self-renew in response to basic fibroblast growth factor. *J Neurosci*. 1996;16(3):1091–1100.
13. Chong YK, Toh TB, Zaiden N, et al. Cryopreservation of neurospheres derived from human glioblastoma multiforme. *Stem Cells*. 2009;27(1):29–39.
14. Clavreul A, Soulard G, Lemee JM, et al; FGB network. The French glioblastoma biobank (FGB): a national clinicobiological database. *J Transl Med*. 2019;17(1):133.
15. Minami JK, Morrow D, Bayley NA, et al. CDKN2A deletion remodels lipid metabolism to prime glioblastoma for ferroptosis. *Cancer Cell*. 2023;41(6):1048–1060.e9.
16. Zhang J, Straehle J, Joseph K, et al. Isolation and profiling of viable tumor cells from human ex vivo glioblastoma cultures through single-cell transcriptomics. *STAR Protoc*. 2023;4(3):102383.
17. Hubert CG, Rivera M, Spangler LC, et al. A Three-dimensional organoid culture system derived from human glioblastomas recapitulates the hypoxic gradients and cancer stem cell heterogeneity of tumors found in vivo. *Cancer Res*. 2016;76(8):2465–2477.
18. LeBlanc VG, Trinh DL, Aslanpour S, et al. Single-cell landscapes of primary glioblastomas and matched explants and cell lines show variable retention of inter- and intratumor heterogeneity. *Cancer Cell*. 2022;40(4):379–392.e9.
19. Jacob F, Salinas RD, Zhang DY, et al. A patient-derived glioblastoma organoid model and biobank recapitulates inter- and intra-tumoral heterogeneity. *Cell*. 2020;180(1):188–204.e22.
20. Pine AR, Cirigliano SM, Nicholson JG, et al. Tumor microenvironment is critical for the maintenance of cellular states found in primary glioblastomas. *Cancer Discov*. 2020;10(7):964–979.

21. Louis DN, Perry A, Wesseling P, et al. The 2021 WHO classification of tumors of the central nervous system: a summary. *Neuro Oncol.* 2021;23(8):1231–1251.
22. Bhat KPL, Balasubramaniyan V, Vaillant B, et al. Mesenchymal differentiation mediated by NF-kappaB promotes radiation resistance in glioblastoma. *Cancer Cell.* 2013;24(3):331–346.
23. Carro MS, Lim WK, Alvarez MJ, et al. The transcriptional network for mesenchymal transformation of brain tumours. *Nature.* 2010;463(7279):318–325.
24. Chanoch-Myers R, Wider A, Suva ML, Tirosh I. Elucidating the diversity of malignant mesenchymal states in glioblastoma by integrative analysis. *Genome Med.* 2022;14(1):106.
25. Garcia-Alonso L, Holland CH, Ibrahim MM, Turei D, Saez-Rodriguez J. Benchmark and integration of resources for the estimation of human transcription factor activities. *Genome Res.* 2019;29(8):1363–1375.
26. Tan MSY, Sandanaraj E, Chong YK, et al. A STAT3-based gene signature stratifies glioma patients for targeted therapy. *Nat Commun.* 2019;10(1):3601.
27. Zhao K, Cui X, Wang Q, et al. RUNX1 contributes to the mesenchymal subtype of glioblastoma in a TGFbeta pathway-dependent manner. *Cell Death Dis.* 2019;10(12):877.
28. de Souza CF, Sabedot TS, Malta TM, et al. A distinct DNA methylation shift in a subset of glioma CpG Island methylator phenotypes during tumor recurrence. *Cell Rep.* 2018;23(2):637–651.
29. Yamini B. NF-kappaB, mesenchymal differentiation and glioblastoma. *Cells.* 2018;7(9):125.
30. Lee DW, Ramakrishnan D, Valenta J, et al. The NF-kappaB RelB protein is an oncogenic driver of mesenchymal glioma. *PLoS One.* 2013;8(2):e57489.
31. Wang L, Babikir H, Muller S, et al. The phenotypes of proliferating glioblastoma cells reside on a single axis of Variation. *Cancer Discov.* 2019;9(12):1708–1719.
32. Richards LM, Whitley OKN, MacLeod G, et al. Gradient of Developmental and Injury Response transcriptional states defines functional vulnerabilities underpinning glioblastoma heterogeneity. *Nat Cancer.* 2021;2(2):157–173.
33. Segerman A, Niklasson M, Haglund C, et al. Clonal variation in drug and radiation response among glioma-initiating cells is linked to proneural-mesenchymal transition. *Cell Rep.* 2016;17(11):2994–3009.
34. Newman AM, Steen CB, Liu CL, et al. Determining cell type abundance and expression from bulk tissues with digital cytometry. *Nat Biotechnol.* 2019;37(7):773–782.
35. Muller S, Kohanbash G, Liu SJ, et al. Single-cell profiling of human gliomas reveals macrophage ontogeny as a basis for regional differences in macrophage activation in the tumor microenvironment. *Genome Biol.* 2017;18(1):234.
36. Chen Z, Soni N, Pinero G, et al. Monocyte depletion enhances neutrophil influx and proneural to mesenchymal transition in glioblastoma. *Nat Commun.* 2023;14(1):1839.
37. Gutmann DH, Kettenmann H. Microglia/brain macrophages as central drivers of brain tumor pathobiology. *Neuron.* 2019;104(3):442–449.
38. Ajaib S, Lodha D, Pollock S, et al. GBMdeconvoluteR accurately infers proportions of neoplastic and immune cell populations from bulk glioblastoma transcriptomics data. *Neuro Oncol.* 2023;25(7):1236–1248.
39. Wei J, Chen P, Gupta P, et al. Immune biology of glioma-associated macrophages and microglia: functional and therapeutic implications. *Neuro Oncol.* 2020;22(2):180–194.
40. Ghoshdastider U, Rohatgi N, Mojtabavi Naeini M, et al. Pan-cancer analysis of ligand-receptor cross-talk in the tumor microenvironment. *Cancer Res.* 2021;81(7):1802–1812.
41. Schmitt MJ, Company C, Dramaretska Y, et al. Phenotypic mapping of pathologic cross-talk between glioblastoma and innate immune cells by synthetic genetic tracing. *Cancer Discov.* 2021;11(3):754–777.
42. Chen P, Zhao D, Li J, et al. Symbiotic macrophage-glioma cell interactions reveal synthetic lethality in PTEN-null glioma. *Cancer Cell.* 2019;35(6):868–884.e6.
43. Yu W, Gui S, Peng L, et al. STAT3-controlled CHI3L1/SPP1 positive feedback loop demonstrates the spatial heterogeneity and immune characteristics of glioblastoma. *Dev Cell.* 2025;60(12):1751-1767.e9.
44. Binda E, Visioli A, Giani F, et al. Wnt5a drives an invasive phenotype in human glioblastoma stem-like cells. *Cancer Res.* 2017;77(4):996–1007.
45. Hu B, Wang Q, Wang YA, et al. Epigenetic activation of WNT5A drives glioblastoma stem cell differentiation and invasive growth. *Cell.* 2016;167(5):1281–1295.e18.
46. Johnson KC, Anderson KJ, Courtois ET, et al. Single-cell multimodal glioma analyses identify epigenetic regulators of cellular plasticity and environmental stress response. *Nat Genet.* 2021;53(10):1456–1468.
47. Wu B, Wang W, Wang H, et al. Single-cell sequencing of glioblastoma reveals central nervous system susceptibility to SARS-CoV-2. *Front Oncol.* 2020;10:566599.
48. Yu K, Hu Y, Wu F, et al. Surveying brain tumor heterogeneity by single-cell RNA-sequencing of multi-sector biopsies. *Natl Sci Rev.* 2020;7(8):1306–1318.
49. Zhao W, Dovas A, Spinazzi EF, et al. Deconvolution of cell type-specific drug responses in human tumor tissue with single-cell RNA-seq. *Genome Med.* 2021;13(1):82.
50. Yan T, Tan Y, Deng G, et al. TGF-beta induces GBM mesenchymal transition through upregulation of CLDN4 and nuclear translocation to activate TNF-alpha/NF-kappaB signal pathway. *Cell Death Dis.* 2022;13(4):339.
51. Kim Y, Varn FS, Park SH, et al. Perspective of mesenchymal transformation in glioblastoma. *Acta Neuropathol Commun.* 2021;9(1):50.
52. McDermott MF. TNF and TNFR biology in health and disease. *Cell Mol Biol (Noisy-le-grand).* 2001;47(4):619–635.
53. Guo Q, Shen S, Guan G, et al. Cancer cell intrinsic TIM-3 induces glioblastoma progression. *iScience.* 2022;25(11):105329.
54. Peng P, Zhu H, Liu D, et al. TGFBI secreted by tumor-associated macrophages promotes glioblastoma stem cell-driven tumor growth via integrin alphavbeta5-Src-Stat3 signaling. *Theranostics.* 2022;12(9):4221–4236.
55. Shi Y, Ping YF, Zhou W, et al. Tumour-associated macrophages secrete pleiotrophin to promote PTPRZ1 signalling in glioblastoma stem cells for tumour growth. *Nat Commun.* 2017;8(1):15080.
56. Wang W, Li T, Cheng Y, et al. Identification of hypoxic macrophages in glioblastoma with therapeutic potential for vasculature normalization. *Cancer Cell.* 2024;42(5):815–832.e12.
57. Zhang Y, Kang T, Wang Y, et al. A low level of tumor necrosis factor alpha in tumor microenvironment maintains the self-renewal of glioma stem cells by Vasorin-mediated glycolysis. *Neuro Oncol.* 2024;26(12):2256–2271.
58. Zhou W, Ke SQ, Huang Z, et al. Periostin secreted by glioblastoma stem cells recruits M2 tumour-associated macrophages and promotes malignant growth. *Nat Cell Biol.* 2015;17(2):170–182.
59. Tanner G, Barrow R, Ajaib S, et al. IDHwt glioblastomas can be stratified by their transcriptional response to standard treatment, with implications for targeted therapy. *Genome Biol.* 2024;25(1):45.
60. Zhang Y, Wong CY, Lim CZJ, et al. Multiplexed RNA profiling by regenerative catalysis enables blood-based subtyping of brain tumors. *Nat Commun.* 2023;14(1):4278.
61. Cheng HS, Chong YK, Lim EKY, et al. Dual p38MAPK and MEK inhibition disrupts adaptive chemoresistance in mesenchymal glioblastoma to temozolomide. *Neuro-Oncology.* 2024;26(7):1247–1261.
62. Koh LWH, Pang QY, Novera W, et al. EZH2 functional dichotomy in reactive oxygen species-stratified glioblastoma. *Neuro Oncol.* 2025;27(2):398–414.
63. Lee J, Kotliarova S, Kotliarov Y, et al. Tumor stem cells derived from glioblastomas cultured in bFGF and EGF more closely mirror the phenotype

and genotype of primary tumors than do serum-cultured cell lines. *Cancer Cell*. 2006;9(5):391–403.
64. Junk DJ, Bryson BL, Smigiel JM, et al. Oncostatin M promotes cancer cell plasticity through cooperative STAT3-SMAD3 signaling. *Oncogene*. 2017;36(28):4001–4013.
65. Weis J, Schonrock LM, Zuchner SL, et al. CNTF and its receptor subunits in human gliomas. *J Neurooncol*. 1999;44(3):243–253.
66. Heinrich PC, Behrmann I, Muller-Newen G, Schaper F, Graeve L. Interleukin-6-type cytokine signalling through the gp130/Jak/STAT pathway. *Biochem J*. 1998;334 (Pt 2)(Pt 2):297–314.
67. Winkles JA, Tran NL, Brown SA, et al. Role of TWEAK and Fn14 in tumor biology. *Front Biosci*. 2007;12(1):2761–2771.
68. Chicheportiche Y, Bourdon PR, Xu H, et al. TWEAK, a new secreted ligand in the tumor necrosis factor family that weakly induces apoptosis. *J Biol Chem*. 1997;272(51):32401–32410.
69. Brown SA, Richards CM, Hanscom HN, Feng SL, Winkles JA. The Fn14 cytoplasmic tail binds tumour-necrosis-factor-receptor-associated factors 1, 2, 3 and 5 and mediates nuclear factor-kappaB activation. *Biochem J*. 2003;371(Pt 2):395–403.
70. Saitoh T, Nakayama M, Nakano H, et al. TWEAK induces NF-kappaB2 p100 processing and long lasting NF-kappaB activation. *J Biol Chem*. 2003;278(38):36005–36012.
71. Hersh DS, Harder BG, Roos A, et al. The TNF receptor family member Fn14 is highly expressed in recurrent glioblastoma and in GBM patient-derived xenografts with acquired temozolomide resistance. *Neuro Oncol*. 2018;20(10):1321–1330.
72. Connolly NP, Galisteo R, Xu S, et al. Elevated fibroblast growth factor-inducible 14 expression transforms proneural-like gliomas into more aggressive and lethal brain cancer. *Glia*. 2021;69(9):2199–2214.
73. Li G, Zhang Z, Cai L, et al. Fn14-targeted BiTE and CAR-T cells demonstrate potent preclinical activity against glioblastoma. *Oncoimmunology*. 2021;10(1):1983306.
74. Brenner D, Blaser H, Mak TW. Regulation of tumour necrosis factor signalling: live or let die. *Nat Rev Immunol*. 2015;15(6):362–374.
75. Belenguer G, Duart-Abadia P, Jordan-Pla A, et al. Adult neural stem cells are alerted by systemic inflammation through tnf-alpha receptor signaling. *Cell Stem Cell*. 2021;28(2):285–299.e9.
76. Vredevoogd DW, Kuilman T, Ligtenberg MA, et al. Augmenting Immunotherapy Impact by Lowering Tumor TNF Cytotoxicity Threshold. *Cell*. 2020;180(2):404–405.
77. Tomolonis JA, Xu X, Dholakia KH, et al. Interaction between tumor cell TNFR2 and monocyte membrane-bound TNF-alpha triggers tumorigenic inflammation in neuroblastoma. *J ImmunoTher Cancer*. 2023;11(3):e005478.
78. Novak M, Majc B, Malavolta M, et al. The Slovenian translational platform GlioBank for brain tumor research: Identification of molecular signatures of glioblastoma progression. *Neurooncol. Adv.*. 2025;7(1):vdaf015.
79. Peng T, Ma X, Hua W, et al. Individualized patient tumor organoids faithfully preserve human brain tumor ecosystems and predict patient response to therapy. *Cell Stem Cell*. 2025;32(4):652–669.e11.
80. Mangena V, Chanoch-Myers R, Sartore R, et al. Glioblastoma cortical organoids recapitulate cell-state heterogeneity and intercellular transfer. *Cancer Discov*. 2025;15(2):299–315.